Heat Capacity and Thermodynamic Functions of di-,tri- and tetramethylammonium lead iodide perovskites from 289 to 473 K

S. Vecchio Ciprioti (Conceptualization) (Formal analysis) (Funding acquisition) (Writing - original draft) (Writing - review and editing), A. Ciccioli (Conceptualization) (Formal analysis) (Funding acquisition) (Investigation) (Methodology) (Writing - original draft) (Writing - review and editing), M.L. Mele (Data curation) (Investigation) (Methodology), P. Russo (Data curation) (Investigation) (Methodology), G. Pulci (Data curation) (Investigation), A. Latini (Data curation) (Funding acquisition) (Investigation) (Writing - original draft)

PII: S0040-6031(19)31056-1

DOI: https://doi.org/10.1016/j.tca.2020.178583

Reference: TCA 178583

To appear in: *Thermochimica Acta*

Received Date: 23 November 2019

Revised Date: 5 March 2020

Accepted Date: 6 March 2020

Please cite this article as: Vecchio Ciprioti S, Ciccioli A, Mele ML, Russo P, Pulci G, Latini A, Heat Capacity and Thermodynamic Functions of di-,tri- and tetramethylammonium lead iodide perovskites from 289 to 473 K, *Thermochimica Acta* (2020), doi: https://doi.org/10.1016/j.tca.2020.178583

Heat Capacity and Thermodynamic Functions of di-,tri- and tetramethylammonium lead iodide perovskites from 289 to 473 K

S. Vecchio Ciprioti[a,*], A. Ciccioli[b], M. L. Mele[c], P. Russo[c], G. Pulci[c,d], A. Latini[b]

[a] Department of Basic and Applied Science for Engineering, Sapienza University of Rome, Via del Castro Laurenziano 7, I-00161 Rome, Italy
[b] Department of Chemistry, Sapienza University of Rome, P.le A, Moro 5, I-00185 Rome, Italy
[c] Department of Chemical Engineering, Materials, Environment, Sapienza University of Rome, Via Eudossiana 18, I-00184 Rome, Italy
[d] INSTM Reference Laboratory for Engineering of Surface Treatments, Via Eudossiana 18, Rome 00184, Italy

e-mail: stefano.vecchio@uniroma1.it

ORCID: Stefano Vecchio Ciprioti (0000-0002-7864-4266); Andrea Ciccioli (0000-0003-1421-8062); Maria Luisa Mele (0000-0003-0594-0248); Paola Russo (0000-0001-6877-6356); Giovanni Pulci (0000-0001-8345-4419); Alessandro Latini (0000-0002-3205-482)

Highlights

- Morphology of di, tri and tetramethylammonium lead iodides was studied by SEM
- Phase purities of the newly synthesized perovskites was checked by XRD
- Cp data on these lead iodides perovskites have been determined by DSC
- Numerical integration of Cp data provided increments of thermodynamic enthalpies and entropies
- A phase transition occurred on tri and tetramethylammonium lead iodides at 347.1 and 353.1 K

Abstract. The heat capacity of di-, tri- and tetramethylammonium lead iodide perovskites of general formula $(CH_3)_xNH_{4-x}PbI_3$ (where $2 \leq x \leq 4$) has been determined by differential scanning calorimetry (DSC) in the temperature range 289–473 K using the step-scan mode. Standard molar values C^0_p(298 K) of di-, tri- and tetramethylammonium lead iodide perovskites were found to be: (285.2, 318.8 and 363.4) J K^{-1} mol^{-1}, respectively. Heat capacity data have been used to evaluate the thermodynamic functions of the three $(CH_3)_xNH_{4-x}PbI_3$ perovskites (entropy and enthalpy increment). Further DSC experiments were carried out simultaneously with thermogravimetry (TG) at constant heating rate (4 K min^{-1}) to study the thermal behavior. The occurrence of a phase transition was detected in two of the three perovskites in well-defined temperature ranges and the corresponding transition temperatures (taken as the onset temperatures of the DSC peaks) resulted to be 346.6 K and 353.5 K for $(CH_3)_3NHPbI_3$ and $(CH_3)_4NPbI_3$, respectively. The three powder samples were also characterized by X-ray diffraction (XRD) and scanning electron microscopy (SEM) analyses.

Keywords: Heat capacity, Differential scanning calorimetry, Thermodynamic functions, X-ray diffraction, Scanning electron microscopy, Alkylammonium lead halide perovskites

1. Introduction

Hybrid lead halide perovskites, especially methylammonium lead iodide $CH_3NH_3PbI_3$, attracted great attention by the scientific community as light absorbers in photovoltaic devices because of their outstanding performances in thin film solar cells and the relatively simple manufacturing process [1-3]. A conversion efficiency value of 23.7% was recently attained, comparable with the best crystalline Si based devices [4], but the lack of long-term stability of these materials in the devices still precludes their commercial debut and, until a viable solution to the stability issues will be found, this debut cannot be envisaged. The instability of $CH_3NH_3PbI_3$ and related perovskites has been extensively studied experimentally with both microscopic (spectroscopic, diffractometric and electrochemical techniques) [5-7] and macroscopic approaches through classical thermodynamics [8-11], as well as with theoretical calculations [12-14]. The macroscopic approach is presented in a much smaller number of literature studies compared to the microscopic approach and theoretical calculations [15], and this is quite surprising, considering the fact that a complete thermodynamic characterization of a material is necessary to assess its stability in the different conditions it encounters. Microscopic approach cannot give thermodynamic stability data; in the best cases only apparent kinetic parameters can be obtained, while theoretical calculations alone may not be sufficiently accurate to obtain reliable thermodynamic data, considering the approximations involved in the procedure. Such a lack of experimental thermodynamic data may be justified by considering the limited number of research groups operating in the field worldwide and by the intrinsic problems of these kind of measurements, experimentally difficult and very time consuming. In fact, simple thermochemical (i.e. calorimetric) measurements are not at all sufficient to assess the stability of a material, being the ΔG and not the ΔH (at constant temperature and pressure) that determines the spontaneity of a process. The necessity of obtaining free energy values usually requires the use of a combination of techniques like tensimetric and calorimetric

measurements. By using these techniques, the complete thermodynamic characterization of $CH_3NH_3PbI_3$ formation and thermal decomposition process was obtained [8-10] and, using these data, the stability of the material in a variety of condition can be determined. The Achilles' heel of $CH_3NH_3PbI_3$ is the Brönsted acidity of the $CH_3NH_3^+$, which accounts for both the thermal instability and the water sensitivity of the material. In fact, it was recently demonstrated that using a quaternary ammonium cation, without acidic hydrogen atoms, it is possible to obtain thermally and water resistant perovskites [11].

On the other hand, the knowledge of the changes in the thermodynamic quantities during the occurrence of transitions is of great importance in the study of the stability of any kind of materials. Many authors focused their attention on determining the thermodynamic properties of their solid-to-solid and solid-to-liquid phase transitions [16-18], molar heat capacities and fusion thermodynamic properties to get close information on intermolecular forces and crystal packing arrangements [19-23].

The aim of this study was to measure the isobaric heat capacity of the three di-, tri- and tetramethylammonium lead perovskites of general formula $(CH_3)_xNH_{4-x}PbI_3$ (where $2 \leq x \leq 4$) and determine the thermodynamic functions in the temperature range 289–473 K using differential scanning calorimetry (DSC), after a morphological and structural characterization of the powder samples performed by X-ray diffraction (XRD) and scanning electron microscopic (SEM) analyses.

2. Experimental

2.1. Materials

The three materials were synthesized according to the procedures reported elsewhere [11,24,25]. The appearance of the solid samples (before kindly grinding them in an agate mortar to perform all measurements) is reported in Fig. 1a-c, where $(CH_3)_2NH_2PbI_3$ sample is yellow-gray, $(CH_3)_3NHPbI_3$ is yellow-gold and $(CH_3)_4NPbI_3$ is very pale yellow). The source, initial purity (for lead acetate trihydrate and tetramethylammonium iodide) or concentration (for hydriodic acid,

dimethylamine and trimethylamine aqueous solutions) and final purities (for di-, tri- and tetramethylammonium lead iodides), all expressed as mass fractions, are reported in Table 1. Purity for reagents was reported as indicated by the supplier, while the final purity for the perovskites tested was checked by XRD. To check the elemental composition of the perovskites, elemental analyses for C, H, and N were provided by the *Servizio di Microanalisi* of the Department of Chemistry of Sapienza University of Rome (Italy) by using an EA 1110 CHNS-O instrument. The results obtained were summarized in Table 2, where the agreement with the expected elemental content is excellent, thus confirming the calculated formulas.

2.2. Instruments

2.2.1. Structural and morphological measurements (XRD and SEM analyses)

Powder X-ray diffraction patterns were obtained using a Panalytical X'Pert Pro MPD diffractometer (Cu Kα source, λ = 1.54184 Å). The diffractometer is equipped with an ultrafast X'Celerator RTMS detector (angular resolution in 2θ = 0.0011, 0.04 rad soller slit, 1° divergence slit, 20 mm mask on the incident beam path; 6.6 mm anti-scatter slit, Ni Kβ filter, 0.04 rad collimator have been used on the diffracted beam path).

Morphology was investigated using a FEG-SEM MIRA3, TESCAN (Brno, Czech Republic) equipped with a SE/BSE detector. The powder samples were observed as such, without metallization or other treatments.

2.2.2. Thermal behavior study

The thermal behavior of the three compounds was studied using two different apparatuses at constant heating rate. To check the occurrence of any mass loss up to 673 K, and to associate it (if any) to endo or exothermic effects a simultaneous Stanton Redcroft (STA625 model) Thermogravimetry (TG)/Heat Flux Differential Thermal Analysis (hfDTA) equipment was used. After calibration with sapphire this instrument is able to provide heat flow data as a DSC apparatus

(with lower sensitivity). So, this unit was used as a simultaneous TG/DSC apparatus that provides both the mass change and the heat flow as a function of time/temperature under a given temperature program. The instrument is equipped with two Al crucibles (one for the sample and one for the reference, which was empty). About 15 mg of each sample, precisely weighed with accuracy of ±0.001 mg, was considered with purging inert Ar atmosphere of 50 ml min^{-1} and heating rate of 4 K min^{-1}. Calibration of temperature was performed by measuring the onset melting temperatures of high purity indium and zinc. Calibration of heat flow has been checked by comparison of the enthalpies of fusion of the same metals (agreement was found within 4%).

Nevertheless, more accurate calorimetric measurements were carried out from 287 to 523 K by using a conventional Perkin Elmer DSC equipment (model 8500) using crimped Al pans at a heating rate of 2 K min^{-1} under nitrogen flow at 20 ml min^{-1}. The calibration procedure used for this instrument was the same as described above for the hfDTA unit.

2.2.3. Heat capacity measurements

Heat capacity data were determined for the three $(CH_3)_xNH_{3-x}PbI_3$ perovskites by using the above mentioned Perkin Elmer 8500 DSC apparatus under a different temperature program: the so-called step-scan mode. This program provides information essentially equivalent to that obtainable by a temperature-modulated DSC [26]. This technique can separate the thermodynamic effect (reversing specific heat) and kinetic effect (non reversing heat flow due to cold crystallization, recrystallization, reorganization during melting, etc.). With a StepScan software program provided by the manufacturer, after a 10 minutes isothermal step at 287 K, we repeated 2K steps of heating at 10 K min^{-1} with 118 repetitions followed by another isothermal step at 483 K for 10 minutes. To take into account the presence of the aluminum pan, its heat capacity at each temperature and the slight difference between the sample and the reference crucible a correction factor *FC* was subtracted to the estimate of the actual $C^0_p(T)$ values of the sample, calculated as follows [24]:

$FC = C^0_p$ (Al) [(pan weight + sample weight) – (reference pan weight)]/sample weight

where the C^0_p (Al) was calculated according to the following formula [25]:

C^0_p (Al) = (4.8 + 0.00322T).

3. Results and discussion

3.1. Structural and morphological characterization by XRD and SEM

X-ray diffraction patterns of dimethylammonium, trimethylammonium and tetramethylammonium lead iodides are reported in Fig. 2a-c, respectively. The patterns are in perfect agreement with literature data, displaying only the reflection of the respective three compounds [11, 27, 28], with no detectable impurities. Consequently the compounds are >99% wt. pure, considering the detection limit of the technique. The purity of the reactants used and of the produced compounds are summarized in Table 1. Their morphology was investigated by analyzing the corresponding SEM images shown in Fig. 3a-c. The SEM image of $(CH_3)_2NH_2PbI_3$ (Fig. 3a) shows an evident bimodal granulometric size distribution, characterized by few 50 µm particles, while the typical size is under 20 µm, and many finer particles were also detected. $(CH_3)_3NHPbI_3$ sample showed in Fig. 3b a considerably more rounded morphology, accompanied by a less unbalanced bimodal size distribution, with larger particles of around 30 µm and a fine fraction of about 10 µm. Finally, the morphology of $(CH_3)_4NPbI_3$ is extremely defined and peculiar (Fig. 3c): elongated particles with a diameter smaller than 2-5 µm and larger diameter from about 5 to 50 µm. No particles of different morphology were observed for this sample.

3.2. Thermal behavior study

The TG/DSC (actually derived from hfDTA) curves of the three perovskites are shown in Fig. 4a-b. No detectable mass loss is observed for all the three compounds up to about 500 K. No evident endo or exothermic effect is observed in the hfDSC curve of $(CH_3)_2NH_2PbI_3$ in the same temperature range, while two very small endothermic effects are found for $(CH_3)_3NHPbI_3$ and $(CH_3)_4NPbI_3$, whose onset temperatures are (345.7 ± 0.8) and (353.3 ± 0.8) K, respectively, where

these uncertainties are standard ones (see the black circle with dotted lines in the inner plot). The thermal behavior of $(CH_3)_4NPbI_3$ has been recently studied by our group in this temperature range using a conventional DSC equipment under both constant heating and cooling rate [11]. In that work a reversible phase transition was observed at 355.1 K (onset temperature) with practically no hysteresis. The XRD pattern registered for this phase at 400 K (well above the transition temperature range) resulted to be equal to that obtained at room temperature, with no new phase formed. On the basis of the above evidences, this transition was tentatively proposed to have a second-order character [11]. At higher temperature all the compounds investigated underwent a thermal decomposition with mass loss higher than 25%, and on the basis of the corresponding onset temperatures (543.9, 571.0 and 639.0 K for $(CH_3)_2NH_2PbI_3$, $(CH_3)_3NHPbI_3$ and $(CH_3)_4NPbI_3$, respectively) the following relative stability scale can be assessed: $(CH_3)_2NH_2PbI_3$ < $(CH_3)_3NHPbI_3$ < $(CH_3)_4NPbI_3$. As a result, it seems evident that the more is the number of methyl groups in the ammonium cation the higher is the thermal stability of the corresponding perovskite.

In order to have a close insight into the phase transitions occurring at low temperature for two of the three compounds tested further DSC experiments were carried out at low heating rate (2 K min^{-1}) with a new Perkin Elmer apparatus (see details in the Experimental section). The DSC curves of the three perovskites are shown in Fig. 5. These new measurements evidently confirmed the thermal behavior shown by the hfDTA measurements. In particular, no endo/exo effects were observed for $(CH_3)_2NH_2PbI_3$ and the occurrence of the above mentioned phase transitions was confirmed for both $(CH_3)_3NHPbI_3$ and $(CH_3)_4NPbI_3$ at the same temperatures, as detected by hfDTA experiments. The reversible nature of the phase transition for $(CH_3)_3NHPbI_3$ was checked (and confirmed) by carrying out a DSC experiment under constant cooling mode (–2 K min^{-1}), and an exothermic effect was detected at a temperature very close to that of the phase transition. The onset and peak temperatures (T_{on} and T_{peak}, respectively) so determined (under heating mode) are:

$(CH_3)_3NHPbI_3$: T_{on} = (346.6±0.5) K; T_{peak} = (347.1±0.5) K;

$(CH_3)_4NPbI_3$: T_{on} = (353.5±0.5) K; T_{peak} = (355.7±0.5) K.

where the temperature uncertainties are the standard one. It is worth noting that these new values related to the phase transition of $(CH_3)_3NHPbI_3$ and $(CH_3)_4NPbI_3$ are in close agreement with those obtained with the hfDTA (345.7 and 353.3 K, respectively) and, for the latter only, with that recently determined with another DSC apparatus [11]. In view of the better accuracy and precision of the Perkin Elmer 8500 apparatus, we select as the recommended values of the transition temperatures the onset values 346.6 ± 0.5 K and 353.5 ± 0.5 for $(CH_3)_3NHPbI_3$ and $(CH_3)_4NPbI_3$, respectively. The area of the DSC transition peaks was evaluated as 83 ± 3 and 39 ± 3 J mol^{-1} for the tri- and tetramethyl ammonium perovskites. Standard uncertainties were considered for both the temperatures and the area values obtained from DSC experiments.

3.3. Determination of the heat capacity and related thermodynamic functions

The molar heat capacity of the three perovskites investigated was measured in the temperature range 289-473 K by DSC (StepScan method, see details in the Experimental section). These data are given in Tables 3-5 and reported in Fig. 6a-c. Two anomalies are observed for the tri- and tetramethyl ammonium perovskites, corresponding to the phase transitions reported in the previous section. The anomaly in the $C^0_p(T)$ temperature dependence of $(CH_3)_4NPbI_3$ seems to have a λ-shaped appearance.

The experimental heat capacity data were fitted in the range 289-473 K according to the well-known Maier-Kelley equation ($C^0_p(T)$/J K^{-1} $mol^{-1} = a_0 + a_1(T/K) + a_2(T/K)^{-2}$) [29]. It must be stressed that the fitting procedure did not take into account the temperature ranges corresponding to the phase transitions, where the anomaly of the $C^0_p(T)$ would have caused a significant reduction in the goodness of the fit. So, the goodness of the multi-parameter regression procedure has been represented by the parameters reported in Table 6 along with the associated uncertainties.

With regard to the C^0_p values reported in Tables 3-5 we note that they follow, as expected, the number of methyl groups in the ammonium cation and exceed significantly the values reported in literature for the monomethyl substituted perovskite, $CH_3NH_3PbI_3$ [30]. It could be interesting to

compare our experimental values with those estimated by using the well-known Kopp-Neumann empirical rule, which has been largely used for mixed oxide systems, also with perovskite structure [31]. For the compounds under study, the rule should be used in the form, which allows estimating C^0_p for a ABC_c compound from those of the binary precursors AC_{c1} and BC_{c-c1}. Such a comparison can be actually done only for $(CH_3)_4NPbI_3$, the heat capacities of both $(CH_3)_4NI$ and PbI_2 being known in the literature [32,33]. However, the resulting value at 298 K (240 J K^{-1} mol^{-1}) is much lower than that obtained in the present study (363 J K^{-1} mol^{-1}). A similar procedure applied to the $CH_3NH_3SnI_3$ perovskite, for which the heat capacity has been recently reported [34], also results [35] in a large underestimate of the experimental value, whereas it performs better for $CH_3NH_3PbI_3$ [30,35]. On this basis, the application of the Kopp-Neumann additivity scheme to the hybrid perovskites seems not reliable in predicting accurate C^0_p values, although a much larger base of data would be necessary to draw a clear conclusion.

The increment of the standard thermodynamic functions *H* and *S* from the reference temperature 298.15 K were calculated by numerical integration of the heat capacity data. The resulting values are reported in Table 7 as a function of temperature. It is worth noting that the thermodynamic functions reported in Table 7 were derived by integrating the actual experimental C^0_p and C^0_p/T data. The analytical fits of Table 6 and the estimated DSC peak areas were not involved in the calculation.

4. Conclusion

The phase purity of di-, tri- and tetramethylammonium lead iodide perovskites newly synthesized was studied by XRD, while the morphology and thermal behavior was studied by SEM, and simultaneous TG/DSC (actually hfDTA), respectively. No mass loss was observed up to about 500 K, while a phase transition took place in both tri- and tetramethylammonium lead iodides around 350 K. The corresponding characteristic temperatures were determined. At higher temperature all perovskites underwent thermal decomposition, and on the basis of the corresponding onset

temperatures a relative stability scale was assessed: the higher is the number of methyl groups bounded to nitrogen, the higher is the thermal stability. The experimental $C^0_p(T)$ values were calculated in the temperature range 289-473 K by DSC with the StepScan method, and fitted according to the Maier-Kelley equation. The heat capacities at T = 298.15 K, C^0_p(298.15 K), for di-, tri- and tetramethylammonium lead iodide perovskites were found to be, respectively: 285.2, 318.8 and 363.4 J K^{-1} mol^{-1}. Heat capacity values were used to determine the corresponding temperature dependences of the enthalpy and entropy values ($H°(T) - H°$(298.15 K) and $S°(T) - S°$(298.15 K), respectively).

Declaration of Competing Interest

The authors declare that there is no conflict of interest.

Authors Statement

Conceptualization (S. Vecchio Ciprioti, A. Ciccioli); Data curation (M.L. Mele and P. Russo for Cp data, A. Latini for XRD, G. Pulci for SEM); Formal analysis (S. Vecchio Ciprioti, A. Ciccioli); Funding acquisition (A. Latini, A. Ciccioli, S. Vecchio Ciprioti,); Investigation (M.L. Mele and P. Russo for Cp data, A. Ciccioli for Numerical Integration, A. Latini for XRD, G. Pulci for SEM); Methodology (M.L. Mele and P. Russo for Cp data, A. Ciccioli for Interpolation of raw data); Roles/Writing – original draft (A. Latini, S. Vecchio Ciprioti, A. Ciccioli); Writing – review & editing (S. Vecchio Ciprioti, A. Ciccioli).

Acknowledgements

This work was performed in the framework of the Research Project "Sintesi, caratterizzazione e studio della stabilità termodinamica di nuovi sistemi perovskitici ibridi piombo alogenuro" funded by Sapienza University of Rome (2018).

Table 1
Sample table

Chemical Name	Source	Initial mass fraction purity	Purification method	Final mass fraction purity	Analysis method
Lead acetate trihydrate	Alfa Aesar	0.99	None		
Tetramethylammonium iodide	Alfa Aesar	0.99	None		
Hydriodic acid[a]	Alfa Aesar	0.57[b]	None		
Dimethylamine[a]	Alfa Aesar	0.40[b]	None		
Trimethylamine[a]	Alfa Aesar	0.45[b]	None		
Dimethylammonium lead iodide	synthesis		None	> 0.99[c]	X-Ray Diffraction
Trimethylammonium lead iodide	synthesis		None	> 0.99[c]	X-Ray Diffraction
Tetramethylammonium lead iodide	synthesis		Precipitate washing	> 0.99[c]	X-Ray Diffraction

[a]Aqueous solution
[b] Concentration
[c] Phase purity. With regard to the presence of possible volatile impurities, the TG curves showed no mass loss up to 473 K with $u_r = 0.001$ (see Fig. 4).

Table 2

Results of the elemental (C, H, N) analysis (% wt.) of the studied compounds in the crystalline state.[a]

Element	$(CH_3)_2NH_2PbI_3$		$(CH_3)_3NHPbI_3$		$(CH_3)_4NPbI_3$	
	Calc.	Exp.	Calc.	Exp.	Calc.	Exp.
C	3.8	3.8	5.6	5.5	7.3	7.2
H	1.3	1.3	1.6	1.6	1.8	2.0
N	2.2	2.2	2.2	2.1	2.1	2.1

[a] The relative standard uncertainty u_r in the experimental data is ±0.3%.

Table 3

Experimental heat capacity, C^0_p, of $(CH_3)_2NH_2PbI_3$ in the crystalline state at $P = 10^5$ Pa.

T/K[a]	$C^0_p(T)$/J K^{-1} mol^{-1}[b]	T/K	$C^0_p(T)$/J K^{-1} mol^{-1}[b]	T/K	$C^0_p(T)$/J K^{-1} mol^{-1}[b]
289	275.6	343	306.6	413	340.0
291	277.5	348	311.0	418	342.5
293	280.1	353	313.6	423	345.1
295	282.4	358	315.5	428	348.2
297	284.6	363	317.4	433	350.4
298	285.2	368	320.2	438	352.7
303	286.9	373	322.5	443	355.7
308	288.6	378	323.7	448	358.5
313	289.9	383	325.6	453	360.7
318	291.7	388	328.7	458	362.8
323	294.7	393	330.8	463	366.0
328	296.7	398	332.7	468	369.0
333	299.6	403	335.9	473	369.6
338	302.6	408	338.1		

[a] Standard uncertainty $u(T) = \pm 0.1$ K

[b] Relative standard uncertainty $u_r(C°_p) = 0.01$

Table 4

Experimental heat capacity, C^0_p, of $(CH_3)_3NHPbI_3$ in the crystalline state at $P = 10^5$ Pa..

T/K[a]	$C^0_p(T)$/J K^{-1} mol^{-1}[b]	T/K	$C^0_p(T)$/J K^{-1} mol^{-1}[b]	T/K	$C^0_p(T)$/J K^{-1} mol^{-1}[b]
289	309.7	346.0	372.8	378	373.5
291	311.5	346.2	373.0	383	374.8
293	314.9	346.4	373.2	388	376.8
295	317.0	346.6 (T_{trs})	373.4	393	379.6
297	318.5	346.8	373.6	398	381.4
298	318.8	347.0	374.0	403	382.8
303	321.2	347.2	374.3	408	384.4
308	324.3	347.4	374.5	413	385.0
313	328.4	347.6	374.9	418	388.0
318	331.9	347.8	375.2	423	392.1
323	335.2	348	375.6	428	395.6
328	339.4	349	377.1	433	398.6
333	343.0	350	377.9	438	401.4
338	347.1	351	376.3	443	405.9
341	354.5	352	371.0	448	408.6
342	362.1	353	366.3	453	409.8
343	370.2	358	369.0	458	412.2
344	371.4	363	369.6	463	415.9
345	372.1	368	371.3	468	419.8
345.5	372.3	373	373.3	473	425.4

[a] Standard uncertainty $u(T) = \pm 0.1$ K

[b] Relative standard uncertainty $u_r(C°_p) = 0.01$

Table 5

Experimental heat capacity, C^0_p, of $(CH_3)_4NPbI_3$ in the crystalline state at $P = 10^5$ Pa.

T/K[a]	$C^0_p(T)$/J K^{-1} mol^{-1}[,b]	T/K	$C^0_p(T)$/J K^{-1} mol^{-1}[,b]	T/K	$C^0_p(T)$/J K^{-1} mol^{-1}[,b]
289	354.2	352.6	435.4	363	403.1
291	356.8	352.8	435.8	368	402.2
293	359.2	353	436.1	373	402.7
295	360.5	353.2	436.1	378	404.5
297	362.5	353.4	436.1	383	406.5
298	363.4	353.5 (T_{trs})	436.1	388	409.3
303	367.4	353.6	436.0	393	411.7
308	371.6	353.8	435.7	398	412.9
313	374.8	354	435.3	403	416.6
318	380.3	354.2	434.9	408	418.4
323	386.1	354.4	434.3	413	419.1
328	390.2	354.6	433.8	418	423.2
333	396.4	354.8	433.2	423	426.9
338	405.0	355	432.6	428	428.4
343	414.6	355.2	432.0	433	430.2
347	420.9	355.4	431.7	438	434.2
348	423.0	355.6	431.2	443	438.7
349	425.0	355.8	430.6	448	442.8
350	427.2	356	430.1	453	443.8
351	429.8	357	427.3	458	446.1
352	433.6	358	424.3	463	450.3
352.2	434.3	359	420.6	468	453.5
352.4	434.9	360	417.3	473	456.5

[a] Standard uncertainty $u(T) = \pm 0.1$ K

[b] Relative standard uncertainty $u_r(C°_p) = 0.01$

Table 6

Regression parameters for the Maier-Kelley equation:
$C^0_p(T)/\mathrm{J\ K^{-1}\ mol^{-1}} = a_0 + a_1(T/\mathrm{K}) + a_2(T/\mathrm{K})^{-2}$

Regression parameter	$(CH_3)_2NH_2PbI_3$	$(CH_3)_3NHPbI_3$	$(CH_3)_4NPbI_3$
N	186	140	113
a_0	152.80±4.80	215.68±8.27	160.09±7.20
a_1	0.4672±0.0085	0.4634±0.0147	0.6054±0.0128
$a_2\ 10^{-6}$	–0.8047±0.2144	–3.1455±0.3621	1.9587±0.3102
R^2	0.9990	0.9989	0.9988

Table 7

Enthalpy $H°(T) - H°(298.15\ K)$[a] and entropy $S°(T) - S°(298.15\ K)$[b] values of the $(CH_3)_2NH_2PbI_3$, $(CH_3)_3NHPbI_3$, and $(CH_3)_4NPbI_3$perovskites in the crystalline state at $P = 10^5$ Pa.

$(CH_3)_2NH_2PbI_3$			$(CH_3)_3NHPbI_3$			$(CH_3)_4NPbI_3$		
T/K	$H°(T) - H°(298.15K)$ /kJ mol^{-1}	$S°(T) - S°(298.15K)$ /J K^{-1} mol^{-1}	T/K	$H°(T) - H°(298.15K)$ /kJ mol^{-1}	$S°(T) - S°(298.15K)$ /J K^{-1} mol^{-1}	T/K	$H°(T) - H°(298.15K)$ /kJ mol^{-1}	$S°(T) - S°(298.15K)$ /J K^{-1} mol^{-1}
300	0.5284	1.879	300	0.5921	1.977	300	0.6739	2.250
310	3.408	11.30	310	3.831	12.55	310	4.376	14.33
320	6.321	20.54	320	7.133	23.01	320	8.161	26.32
330	9.276	29.63	330	10.50	33.39	330	12.04	38.27
340	12.29	38.62	340	13.99	43.78	340	16.06	50.24
350	15.37	47.55	346.6 (T_{trs})	16.52	50.95	350	20.22	62.31
360	18.51	56.40	350	17.71	54.57	353.5 (T_{trs})	21.74	66.48
370	21.70	65.13	360	21.41	64.99	360	24.47	74.30
380	24.92	73.74	370	25.12	75.16	370	28.56	85.51
390	28.19	82.24	380	28.85	85.11	380	32.61	96.31
400	31.51	90.64	390	32.61	94.88	390	36.69	106.9
410	34.88	98.95	400	36.41	104.5	400	40.81	117.3
420	38.29	107.2	410	40.24	114.0	410	44.98	127.6
430	41.75	115.3	420	44.12	123.2	420	49.20	137.8
440	45.26	123.4	430	48.05	132.5	430	53.47	147.9
450	48.83	131.4	440	52.05	141.7	440	57.80	157.8
460	52.45	139.4	450	56.11	150.9	450	62.19	167.7

470	56.11	147.3	460	60.22	159.9	460	66.64	177.5
			470	64.39	168.9	470	71.15	187.2

[a] Relative standard uncertainty $u_r(H°(T) - H°(298.15\ K)) = 0.02$.

[b] Relative standard uncertainty $u_r(S°(T) - S°(298.15\ K)) = 0.02$.

References

[1] M Grätzel, The Rise of Highly Efficient and Stable Perovskite Solar Cells. Acc. Chem. Res. 50 (2017) 487−491.

[2] Z. Shi, A.H. Jayatissa, Perovskites-Based Solar Cells: A Review of Recent Progress, Materials and Processing Methods. Materials 11 (2018) 729.

[3] A. Kumar Jena, A. Kulkarni, T. Miyasaka, Halide Perovskite Photovoltaics: Background, Status, and Future Prospects. Chem. Rev. 119 (2019) 3036-3103.

[4] M. A. Green, Y. Hishikawa, E.D. Dunlop, D.H. Levi, J. Hohl-Ebinger, M. Yoshita. A.W.Y. Ho-Baillie. Solar cell efficiency tables (Version 53). Prog. Photovolt. Res. Appl. 27 (2019) 3-12.

[5] N.G. Park, M. Grätzel, T. Miyasaka, K. Zhu, K. Emery, Towards stable and commercially available perovskite solar cells. Nat. Energy 1 (2016) 16152.

[6] I. Deretzis, A. Alberti, G. Pellegrino, E. Smecca, F. Giannazzo, N. Sakai, T. Miyasaka, A. La Magna, Atomistic origins of $CH_3NH_3PbI_3$ degradation to PbI_2 in vacuum. Appl. Phys. Lett. 106 (2015) 131904.

[7] K. Domanski, J.P. Correa-Baena, N. Mine, M.K. Nazeeruddin, A. Abate, M. Saliba, W. Tress, A. Hagfeldt, M. Grätzel, Not All That Glitters Is Gold: Metal-Migration-Induced Degradation in Perovskite Solar Cells. ACS Nano 10 (2016) 6306-6314.

[8] B. Brunetti, C. Cavallo, A. Ciccioli, G. Gigli, A. Latini, On the Thermal and Thermodynamic (In)Stability of Methylammonium Lead Halide Perovskites. Sci. Rep. 6 (2016) 31896.

[9] A. Latini, G. Gigli, A. Ciccioli, A study on the nature of the thermal decomposition of methylammonium lead iodide perovskite, $CH_3NH_3PbI_3$: an attempt to rationalise contradictory experimental results. Sustainable Energy Fuels 1 (2017) 1351-1357.

[10] A. Ciccioli, A. Latini, Thermodynamics and the Intrinsic Stability of Lead Halide Perovskites $CH_3NH_3PbX_3$. J. Phys. Chem. Lett. 9 (2018) 3756-3765.

[11] A. Ciccioli, R. Panetta, A. Luongo, Bruno Brunetti, S. Vecchio Ciprioti, Maria Luisa Mele, A. Latini, Stabilizing lead halide perovskites with quaternary ammonium cations: the case of tetramethylammonium lead iodide. Phys. Chem. Chem. Phys. 21 (2019) 24768-24777.

[12] B. Conings, J. Drijkoningen, N. Gauquelin, A. Babayigit, J. D'Haen, L. D'Olieslaeger, A. Ethirajan, J. Verbeeck, J. Manca, E. Mosconi, F. De Angelis, H.G. Boyen, Intrinsic Thermal Instability of Methylammonium Lead Trihalide Perovskite. Adv. Energy Mater. 5 (2015) 1500477.

[13] J.M. Azpiroz, E. Mosconi, J. Bisquert, F. De Angelis, Defect migration in methylammonium lead iodide and its role in perovskite solar cell operation. Energy Environ. Sci. 8 (2015) 2118-2127.

[14] J. Yang, B. D. Siempelkamp, E. Mosconi, F. De Angelis, T.L. Kelly, Origin of the thermal instability in $CH_3NH_3PbI_3$ thin films deposited on ZnO. Chem. Mater. 27 (2015) 4229-4236.

[15] A. Senocrate, G. Y. Kim, M. Grätzel, J. Maier, Thermochemical Stability of Hybrid Halide Perovskites. ACS Energy Lett. 4 (2019) 2859-2870.

[16] E. Badea, I. Blanco, G. Della Gatta, Fusion and solid-to-solid transitions of a homologous series of alkane-α, ω-dinitriles, J. Chem. Thermodyn. 39(10) (2007) 1392-1398.

[17] S. Vecchio, B. Brunetti, Vapor Pressures and Standard Molar Enthalpies, Entropies and Gibbs energies of Sublimation of 2,4- and 3,4-dinitrobenzoic acids. J. Chem. Thermodyn. 41 (2009) 880- 887.

[18] S. Vecchio, M. Tomassetti, Vapor Pressures and Standard Molar Enthalpies, Entropies and Gibbs energies of Sublimation of three 4-substituted acetanilide derivatives. Fluid Phase Equil. 279 (2009) 64-72.

[19] L. Abate, E. Badea, I. Blanco, D. D'Angelo, G. Della Gatta, Heat capacities of a series of terminal linear alkyldiamides determined by DSC, J. Therm. Anal. Calorim. 90 (2007) 575–580.

[20] V.N. Guskov, P.G. Gagarin, A.V. Guskov, A.V. Tyurin, A.V. Khoroshilov, K.S. Gavrichev, Heat capacity and thermal expansion of neodymium hafnate ceramics. Ceram. Int. 45 (2019) 20733–20737.

[21] K. Bryukhanova, G. Nikiforova, A. Khoroshilov, K. Gavrichev, Thermodynamics of $PrPO_4$ whiskers. J. Chem. Thermodyn. 120 (2018) 79–87.

[22] M.G. Bonicelli, A. Catalani, G, Mariano, S. Vecchio, Heat capacities, and molar enthalpies and entropies of fusion for anhydrous 1,10-phenanthroline and 2,9-dimethyl-1,10-phenanthroline. Thermochim. Acta, 466 (2007) 67-71.

[23] A. V. Tyurina, K. S. Gavricheva, A. V. Khoroshilov, and V. P. Zlomanov, Heat Capacity and Thermodynamic Functions of GaSe from 300 to 700 K. Inorg. Mater. 50(3) (2014) 255-258.

[24] PerkinElmer Instruments LLC, StepScan user's manual, October 1999.

[25] D.G. Friend, B.E. Poling, R.L. Rowley, G.H. Thomson, W.V. Wilding, Perry's chemical engineers' handbook, 8th edition, Mc Graw-Hill, 2008.

[26] J. Holubová, E. Cernosková, Z. Cernosek, StepScan DSC. The useful tool for the study of the glass transition phenomenon. J Therm Anal Calorim. 111 (2013) 1633–1638.

[27] A. Mancini, P. Quadrelli, G. Amoroso, C. Milanese, M. Boiocchi, A. Sironi, M. Patrini, G. Guizzetti, L. Malavasi, Synthesis, structural and optical characterization of $APbX_3$ (A = methylammonium, dimethylammonium, trimethylammonium; X = I, Br, Cl) hybrid organic–inorganic materials. J. Solid State Chem. 240 (2016) 55–60.

[28] G. Liu, J. Liu, Z. Sun, Z. Zhang, L. Chang, J. Wang, X. Tao, Q. Zhang, Thermally Induced Reversible Double Phase Transitions in an Organic-Inorganic Hybrid Iodoplumbate $C_4H_{12}NPbI_3$ with Symmetry Breaking. Inorg. Chem. 55 (2016) 8025–8030.

[29] C.G. Maier, K.K. Kelley, An equation for representation of high temperature heat content data, J. Am. Chem. Soc. 54 (1932) 3243–3246.

[30] N. Onoda-Yamamuro, T. Matsuo, H. Suga, Calorimetric and IR spectroscopic studies of phase transitions in methylammonium trihalogenoplumbates (II), J. Phys. Chem. Solids 51 (1990) 1383-1395.

[31] J. Leitner, P. Voňka, D. Sedmidubský, P. Svoboda, Application of Neumann-Kopp rule for the estimation of heat capacity of mixed oxides, Thermochim. Acta 497 (2019) 7-13.

[32] V. S. Iorish, et al., IVTANTHERMO database-Version 3.0., Glushko Thermocenter of Russian Academy of Sciences 2005.

[33] L. V. Coulter, K. S. Pitzer, W. M. Latimer, The entropies of large ions. The heat capacity, entropy and heat of solution of potassium chloroplatinate, tetramethylammonium iodide and uranyl nitrate hexahydrate, J. Am. Chem. Soc. 62 (1940) 2845-2851.

[34] Y. Dang, Y. Zhou, X. Liu, D. Ju, S. Xia, H. Xia, X. Tao, Formation of hybrid perovskite tin iodide single crystals by top-seeded solution growth, Angew. Chem. Int. Ed. 55 (2016) 1-5.

[35] O. Yamamuro, M. Oguni, T. Matsuo, H. Suga, Calorimetric and dilatometric studies on the phase transitions of crystalline CH_3NH_3I. J. Chem. Thermodyn. 18 (10) (1986) 939–954.

Caption of the figures

Fig. 1 Photo of the powder samples of: (a) $(CH_3)_2NH_2PbI_3$, (b) $(CH_3)_3NHPbI_3$ and (c) $(CH_3)_4NPbI_3$

Fig. 2 X-Ray Diffraction patterns of: (a) $(CH_3)_2NH_2PbI_3$, (b) $(CH_3)_3NHPbI_3$ and (c) $(CH_3)_4NPbI_3$

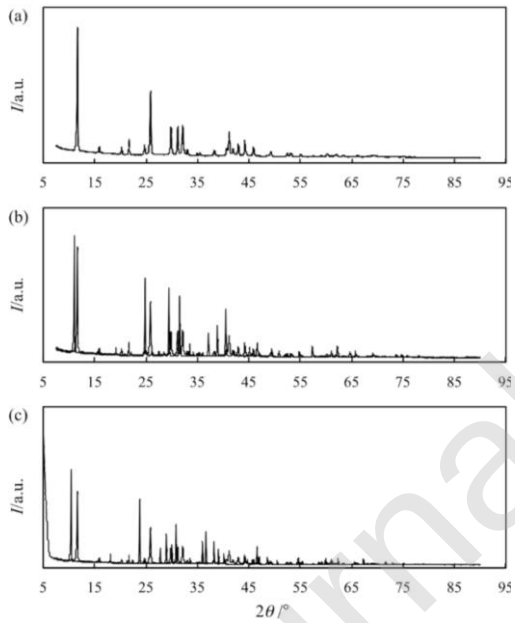

Fig. 3 SEM images (25.0 kV beam voltage, 2.5 kx magnification) of: (a) $(CH_3)_2NH_2PbI_3$, (b) $(CH_3)_3NHPbI_3$ and (c) $(CH_3)_4NPbI_3$. Images a, c and e are obtained with LE-BSE (Low Energy-Back Scattered Electrons). Images b, d and f are obtained with SE (Secondary Electrons).

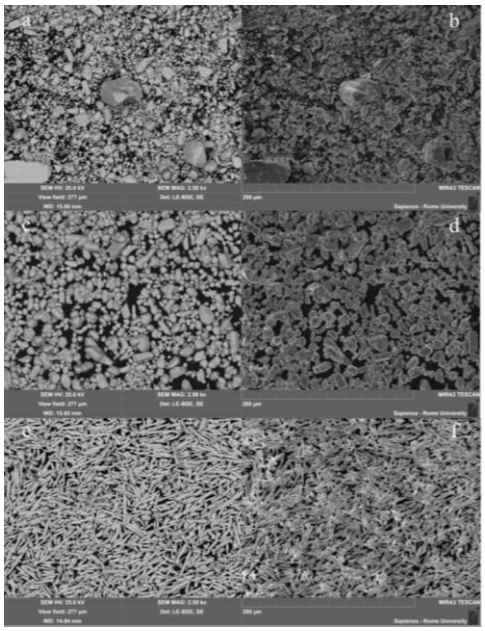

Fig. 4 TG/hfDTA curves of $(CH_3)_2NH_2PbI_3$, $(CH_3)_3NHPbI_3$ and $(CH_3)_4NPbI_3$ under Ar atmosphere at 4 K min^{-1}.

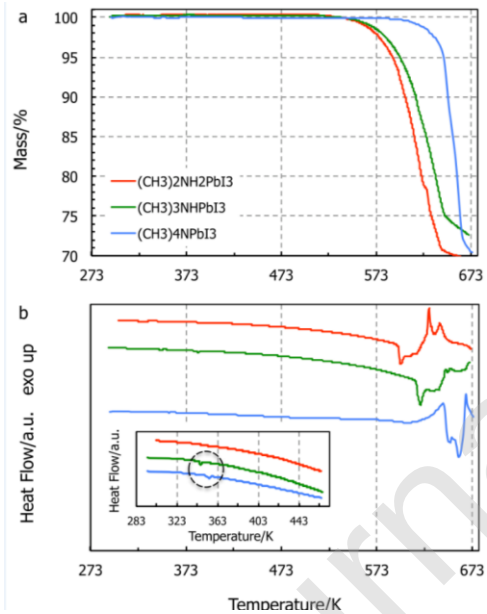

Fig. 5 DSC curves of $(CH_3)_2NH_2PbI_3$, $(CH_3)_3NHPbI_3$ and $(CH_3)_4NPbI_3$ at 2 K min^{-1}

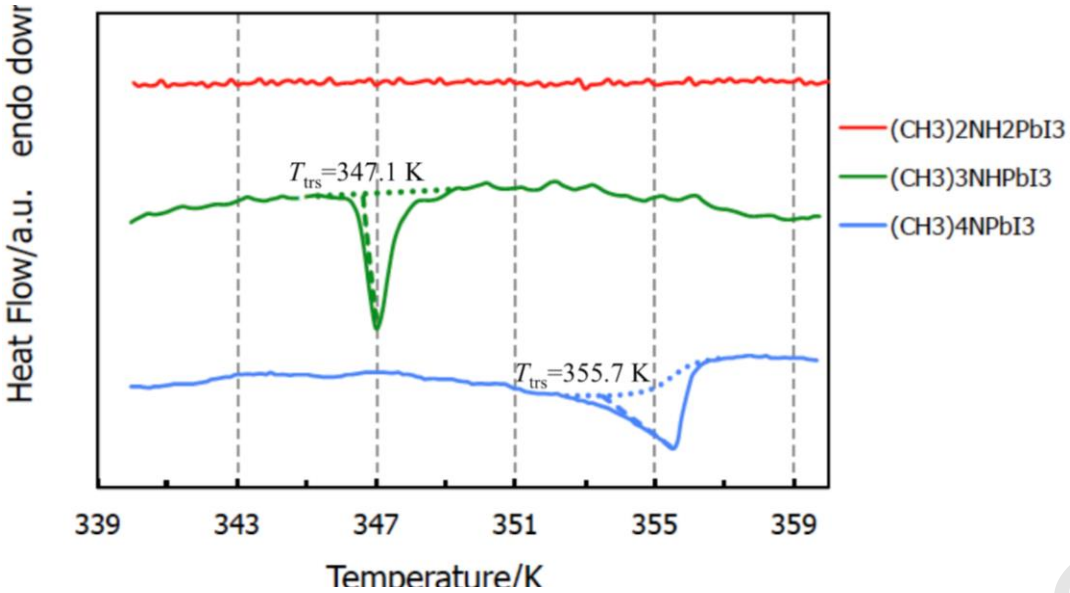

Fig. 6 Temperature dependences of experimental heat capacity data for: (a) $(CH_3)_2NH_2PbI_3$, (b) $(CH_3)_3NHPbI_3$ and (c) $(CH_3)_4NPbI_3$.